1   **High resolution vertical distribution and sources of HONO and NO₂ in the**

2   **nocturnal boundary layer in urban Beijing, China**

4   **Fanhao Meng**[1,2]**, Min Qin**[1]**, Ke Tang**[1,2]**, Jun Duan**[1]**, Wu Fang**[1]**, Shuaixi Liang**[1,2]**, Kaidi Ye**[1,2]**,**

5   **Pinhua Xie**[1,2,3]**, Yele Sun**[3,4,5]**, Conghui Xie**[4]**, Chunxiang Ye**[6]**, Pingqing Fu**[4,*]**, Jianguo Liu**[1,2,3]**,**

6   **Wenqing Liu**[1,2,3]

7   [1]Key Laboratory of Environment Optics and Technology, Anhui Institute of Optics and Fine Mechanics,

8   Chinese Academy of Sciences, Hefei, 230031, China

9   [2]University of Science and Technology of China, Hefei, 230027, China

10   [3]Center for Excellence in Regional Atmospheric Environment, Institute of Urban Environment,

11   Chinese Academy of Sciences, Xiamen, 361021, China

12   [4]State Key Laboratory of Atmospheric Boundary Layer Physics and Atmospheric Chemistry, Institute

13   of Atmospheric Physics, Chinese Academy of Sciences, Beijing, 100029, China

14   [5]University of Chinese Academy of Sciences, Beijing, 100049, China

15   [6]State Key Joint Laboratory of Environmental Simulation and Pollution Control, College of

16   Environmental Sciences and Engineering, Peking University, Beijing, China

17   [*]now at: Institute of Surface-Earth System Science, Tianjing University, Tianjing, 300072, China

18   **Correspondence:** Min Qin (mqin@aiofm.ac.cn)

20   **Abstract.** The production of HONO on aerosol surfaces and ground surfaces in urban atmosphere is of

21   interests. However, ground surface measurement commonly in our society is not able to distinguish

22   these two parts. Here, for the first time, we reported high-resolution vertical profile measurements of

23   HONO and NO₂ in urban Beijing at night using an incoherent broadband cavity enhanced absorption

24   spectrometer (IBBCEAS) amounted on a movable container which attached to a meteorological tower

25   of 325 m high. The mixing ratios of HONO during one haze episode (E1), the clean episode (C2) and

26   another haze episode (E3) were 4.26 ± 2.08, 0.83 ± 0.65, and 3.54 ± 0.91 ppb, respectively.

27   High-resolution vertical profiles revealed that the vertical distribution of HONO is consistent with

28   stratification and layering in the nocturnal urban atmosphere below 250 m. Direct emissions from

29   combustion processes contributed 51.1% to ambient HONO concentration at night. The HONO

30   production from the heterogeneous conversion of NO₂ on the aerosol surfaces cannot explain HONO

31   vertical measurements at night, indicating that the heterogeneous reaction of NO_2 on ground surfaces

32   dominated the nocturnal HONO production. The nocturnal HONO in the boundary layer is primarily

33   derived from the heterogeneous conversion of NO_2 at ground level and direct emissions; it is then

34   transported throughout the column by vertical convection. $\phi_{NO_2 \rightarrow HONO}$, the HONO yield from

35   deposited NO_2, is used to evaluate HONO production from the heterogeneous conversion of NO_2 at

36   night. The derived $\phi_{NO_2 \rightarrow HONO}$ values on 9 (C2), 10 (C2) and 11 December (E3) were 0.10, 0.08, and

37   0.09, respectively, indicating a significant production of HONO from heterogeneous reaction of NO_2 at

38   ground level. The similar $\phi_{NO_2 \rightarrow HONO}$ values measured during clean and haze episodes suggest that

39   the heterogeneous conversion potential of NO_2 at ground level is consistent at night. Furthermore, the

40   dry deposition loss of HONO to the ground surface and vertical mixing effects associated with

41   convection reached a near steady state at midnight on 11-12 December, indicating that significant

42   quantities of HONO are deposited to the ground surface at night, and the ground surface is the source

43   and sink of HONO at night.

44   **1 Introduction**

45   It is well known that the rapid photolysis of HONO (R1) after sunrise is the most important

46   hydroxyl radical (OH) source. 25-90% of daytime OH production was accounted by HONO photolysis

47   according to previous reports (Lu et al., 2012;Ma et al., 2017;Tong et al., 2016;Su et al., 2008b;Huang

48   et al., 2017;Hendrick et al., 2014). OH initiates daytime photochemistry and promotes the formation of

49   secondary products (including ozone (O_3), peroxyacetyl nitrate (PAN)) and secondary aerosols (Alicke

50   and Platt, 2002;Tang et al., 2015;Kleffmann, 2007;An et al., 2012). Besides, there is a growing concern

51   about the possible health effects of the formation of nitrosamines (Hanst et al., 1977;Pitts et al., 1978),

52   in which HONO acts as a nitrosating agent to form carcinogenic nitrosamines (Sleiman et al.,

53   2010;Bartolomei et al., 2015;Gómez Alvarez et al., 2014).

54    $$HONO + h\nu \left(320nm < \lambda < 405nm \right) \rightarrow NO + OH \qquad (R1)$$
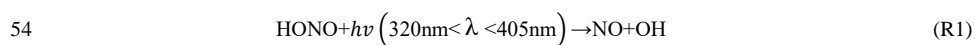
55   Despite the importance of HONO, the details of the formation processes of HONO in the

56   atmosphere remain unclear. Newly available instruments have observed much higher daytime HONO

57   concentrations than simulated values of atmospheric chemical models in both rural and urban areas,

58   implying missing HONO sources (Li et al., 2012;Wang et al., 2017;Oswald et al., 2015;Wong et al.,

59   2012;Li et al., 2014;Liu et al., 2019;Karamchandani et al., 2015;Kleffmann, 2007;Mendez et al.,

60   2017;Michoud et al., 2014;Michoud et al., 2015;Tang et al., 2015;Vogela et al., 2003;Sörgel et al.,

61   2011). Several homogeneous reaction mechanisms for HONO have been proposed but latter have been

62   considered as irrelevant in real atmospheric conditions, including photolysis of ortho-substituted

63   nitroaromatics (Bejan et al., 2006) and the reaction of photoexcited NO_2 with H_2O (Li et al., 2008). In

64   contrast to the homogeneous formation of HONO, the heterogeneous conversion from NO_2 to HONO

65   on humid surfaces (R2) is considered the most likely explanation for the observed HONO

66   concentrations. However, whether the conversion processes primarily occurs on the ground surface or

67   on aerosol surface remains controversial.   (Kleffmann et al., 2003;Su et al., 2008a;Cui et al., 2018;R.

68   Br¨oske et al., 2003;Acker et al., 2006;VandenBoer et al., 2013;Bao et al., 2018;Liu et al., 2014;Meusel

69   et al., 2016;Reisinger, 2000;Tong et al., 2016;Ye et al., 2017). A lot of ground measurements have

70   found significantly positive correlations between HONO and aerosol surface area, suggesting that

71   aerosol surfaces play an important role in the heterogeneous conversion from NO_2 to HONO (Reisinger,

72   2000;Cui et al., 2018;Zhang et al., 2018;Hou et al., 2016;Tong et al., 2016;An et al., 2012). Various

73   chemical compositions both in the soil and on aerosol particle are reactive towards HONO production.

74   Recent laboratory studies have found that reaction of NO_2 and H_2O adsorbed on mineral dust, glass and

75   buildings can produce HONO (Finlayson-Pitts et al., 2003;Ma et al., 2017;Mendez et al., 2017). And

76   the redox reaction of NO_2 has been extensively investigated on the surfaces of soot, mineral dust, and

77   humic acid (Kleffmann et al., 1999;Aubin and Abbatt, 2007;Scharko et al., 2017;Ma et al., 2017). The

78   photosensitized conversion of NO_2 on organic surfaces and emission from biological processes have

79   also been suggested to be a potentially important source of HONO in forested and agricultural region

80   (Gómez Alvarez et al., 2014;Stemmler et al., 2006;Monge et al., 2010;Han et al., 2016;Han et al.,

81   2017;Su et al., 2011;Oswald et al., 2013;Tang et al., 2019;Laufs et al., 2017):
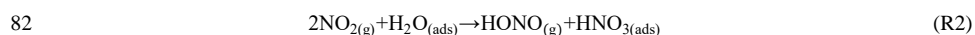
82                          $$2NO_{2(g)}+H_2O_{(ads)} \rightarrow HONO_{(g)}+HNO_{3(ads)} \qquad \text{(R2)}$$

83   While vertical gradients provide direct evidence about the ground and *in situ* HONO formation.

84   The long-path differential optical absorption spectroscopy (LP-DOAS), instruments mounted on the

85   movable elevator of a tall tower or the fixed height of a building and aircraft measurements are the

86   primary HONO vertical gradient measurement methods (Kleffmann et al., 2003;Stutz,

87   2002;VandenBoer et al., 2013;Villena et al., 2011;Wong et al., 2011;Wong et al., 2012;Zhang et al.,

88   2009;Li X et al., 2017;Ye et al., 2018;Li et al., 2014;Oswald et al., 2015;Kleffmann, 2007). Wong et al.

89   (2011) measured the vertical gradients of HONO using LP-DOAS instrument in downtown Houston.

90 The observations showed that NO_2-to-HONO conversion on the ground was the dominant source of

91 HONO, and vertical transport was found to be the primary source of HONO aloft. Similar results were

92 found by Villena et al. (2011), who conducted HONO vertical gradient measurements on the 3rd and

93 21st floor of the high-rise building (6 and 53 m above ground level) in Santiago de Chile. However,

94 these that have been conducted are limited by measurement frequency and vertical resolution between

95 surface and planetary boundary layer (PBL). VandenBoer et al (2013) carried out measurements of high

96 resolution vertical profiles (vertical resolution ~10m over 250m) of HONO on a 300 m triangular

97 open-frame tower. They found that the ground surface HONO production was dominated by

98 heterogeneous uptake of NO_2, and nocturnally deposited HONO may form a conservative surface

99 reservoir which is released on the following day. However, the above HONO vertical gradient

100 observations were predominantly conducted in the lower PBL. In order to understand the important

101 role of HONO photochemistry in troposphere, Zhang et al. (2009) measured HONO vertical profiles

102 using aircraft in the PBL and the lower free troposphere (FT) over a forested region in northern

103 Michigan. The study also found that the ground surface was a major source of HONO in the lower PBL,

104 and the HONO emitted from ground surfaces accounted for 16-27% of the overall HONO in the PBL,

105 most of which was distributed in the lower PBL.

106 Based on the measurement of vertical gradient and HONO flux, most studies suggests the

107 dominate role of HONO formation on the ground surface (Kleffmann et al., 2003;Oswald et al.,

108 2015;VandenBoer et al., 2013;Villena et al., 2011;Wong et al., 2011;Wong et al., 2013;Stutz,

109 2002;Zhang et al., 2009;Meusel et al., 2016;Neuman et al., 2016;Harrison and Kitto, 1994;Harrison et

110 al., 1996), but Cui et al. (2018) also reported evidence for the important role of HONO formation on

111 aerosol. The aerosol mass loading and its chemical composition seem to be a key parameter influencing

112 the relative importance of HONO formation on aerosol surface.

113 Beijing, as the largest and the most densely populated city in China, has suffered from severe haze

114 pollution for several years due to rapid economic development and urbanization. The aerosol surface

115 density has been reported to be 2-3 orders of magnitude higher than typical background area (Cai et al.,

116 2017;Liu et al., 2012;Zhang et al., 2015). And several studies indicated that the increase of secondary

117 aerosols were caused by high levels of OH from photolysis of HONO, which resulted in frequent

118 occurrence of haze pollution (Fu et al., 2019;An et al., 2012;Huang et al., 2014). Several observations

119 of HONO have been conducted in urban and suburban areas of Beijing in recent years (Tong et al.,

120   2016;Zhang et al., 2018;Hou et al., 2016;Wang et al., 2017;Lu et al., 2012;Hendrick et al., 2014).

121   Higher levels of HONO have been observed (up to 9.71 ppb) in Beijing in winter (Spataro et al., 2013)

122   and the contribution of HONO photolysis to OH budget at noon can reach 90% in Beijing in winter

123   (Hendrick et al., 2014). However, most of these studies were conducted at ground level, while the

124   vertical measurements are very limited in Beijing, China.

125   Here, we report the first high-resolution vertical profile measurements of HONO and NO_2 in the

126   megacity of Beijing at different pollution levels (following the transition from the clean episode to haze

127   episode). The vertical profiles of HONO and NO_2 were measured at high vertical resolution (< 2.5 m

128   over 240 m height) between the surface, the nocturnal boundary layer and residual layer. Although the

129   vertical profile measurements are rather limited in scope, including only four nights in December 2016

130   with limited ancillary data, it is unique both because of its high vertical resolution and because of the

131   continuous vertical measurements of HONO and NO_2 at different stage of pollution. Based on the

132   dataset, the heterogeneous formation of HONO on the ground surfaces and aerosol surfaces is

133   investigated. Evidences also suggest HONO deposition at certain atmospheric conditions.

134   **2 Experimental Methods**

135   **2.1 Measurement site**

136   Vertical profile measurements were conducted from 7 to 12 December 2016 at the Tower Branch

137   of the Institute of Atmospheric Physics (IAP), Chinese Academy of Science (39°58'N, 116°23'E) as

138   part of the "In-depth study of air pollution sources and processes within Beijing and its surrounding

139   region (APHH-Beijing)" winter campaign. The site is a typical urban residential area between the 3rd

140   and 4th Ring Road in the north of Beijing. It is approximately 1 km from the 3rd Ring Road; 200 m

141   from the Beijing-Tibet Expressway and 50 m from the Beitucheng West Road (Fig. S1). The main

142   sampling platform is the Beijing 325-m meteorological tower (BMT), equipped with an external

143   container which can ascend and descend at a relatively constant rate of ~ 9 m min^{-1}. A single vertical

144   ascent or descent takes less than 30 min. After reaching the top, the container stopped and data were

145   measured continuously for 5-20 min of each cycle. For security reasons, the container reached a

146   maximum height limit of 260 m during the daytime and 240 m at night (Fig. 1). The container

147   instruments include: a global position system (GPS), an altimeter and an incoherent broadband cavity

148   enhanced absorption spectrometer (IBBCEAS) for measurements of HONO and NO_2. In addition,

149   another IBBCEAS was mounted in temperature-stabilized lab containers for the measurement of

150   HONO and NO_2 at ground level.

2.2 Instrumentation

152   HONO and NO_2 were simultaneously measured by a home-made IBBCEAS. Detailed description

153   of the IBBCEAS instrument can be found in Duan et al (2018); its application to the measurements

154   made during this study is described below. The HONO was sampled into an inlet tube (1.5 m length, 4

155   mm outside diameter (OD)) before entering the optical cavity (550 mm length, 25.4 mm OD), which

156   utilized PFA to minimize the HONO loss. The sampling gas flow rate was controlled at 6 SLPM

157   (Standard Liters per Minute) by a gas pump (KNF). The light emitted by the ultraviolet light-emitting

158   diode (UV-LED) was collimated by achromatic lens and coupled into the optical cavity. In the optical

159   cavity, light was reflected between the two highly reflective mirrors (R = 99.980% @368 nm, CRD

160   Optics, California, USA) to obtain a long optical absorption length. Then the light through the cavity

161   was coupled into an optical fiber by another achromatic lens before being received by a charge coupled

162   device (CCD) spectrometer (QE65000, Ocean Optics, Florida, USA). To protect the highly reflective

163   mirrors, pure N_2 was used to continuously purge the mirrors to prevent contact between the mirrors and

164   sample airflow. The purge flow rate was controlled at 0.1 SLPM by mass flow controllers (MFCs,

165   CS200A, Sevenstar, Beijing, China). The typical time resolution of the IBBCEAS instrument is 30 s,

166   and the 1 σ detection limits for HONO and NO_2 are 90 ppt and 170 ppt, respectively. In this study, the

167   IBBCEAS instrument was mounted in the movable container of the BMT for vertical profile

168   measurements and made measurements with a time resolution of 15 s (vertical resolution of 2.4 m).

169   Another IBBCEAS instrument was mounted in temperature-stabilized lab containers at ground level

170   and collected data with a time resolution of 30 s. The relative measurement error of the IBBCEAS

171   instrument was approximately 9%. Correction of the light intensity was performed every hour, and

172   mirror reflectivity was calibrated every day.

173   Meteorological parameters, including wind speed (WS), wind direction (WD), temperature (*T*),

174   and relative humidity (RH) were obtained using a 15-level meteorological gradient observation system

175   installed at fixed intervals along the meteorological tower (at heights of 8, 15, 32, 47, 65, 80, 100, 120,

176   140, 160, 180, 200, 240, 280 and 320 m). The gaseous species, including nitrogen monoxide (NO),

177   ozone (O_3), carbon monoxide (CO), and sulfur dioxide (SO_2), were measured using commercial gas

178   analyzer from Thermo Scientific. The 7-wavelength aethalometer (AE33, Magee Scientific Corp,

179   Berkeley, USA) was deployed to measure the black carbon (BC) mass concentration. CO, O_3, SO_2, and

180   BC were measured simultaneously at ground level and 260 m on the tower. The non-refractory

181   submicron aerosol (NR-PM$_1$) species were also measured simultaneously at ground level and 260 m on

182   the tower with an Aerodyne high-resolution time-of-flight aerosol mass spectrometer (AMS) and an

183   aerosol chemical speciation monitor (ACSM), respectively. The detailed sampling setup and calibration

184   of the AMS and ACMS as well as data analysis have been described in Xu et al. (2019) and Sun et al.

185   (2013).

2.3 Inter-comparison

187   In the present study, the measurements of HONO and NO_2 were conducted simultaneously in the

188   container and at ground level. Therefore, the calibration and inter-comparison of the two IBBCEAS

189   instruments were crucial. Comparison experiments were carried out in a temperature-stabilized

190   laboratory. The sampling unit and sampling flow rate of the two instruments were identical to minimize

191   the measured deviations. Figure. 2 shows significantly positive correlations between the two IBBCEAS

192   instruments (HONO: $R^2 = 0.99$, NO_2: $R^2 = 0.95$), with a slope of 0.99 (NO_2), 1.03 (HONO) and an

193   intercept of 750 ppt (NO_2) and 4 ppt (HONO). The difference was approximately 3%, within the

194   measurement error range of the instruments.

195   To verify the accuracy of the IBBCEAS instrument, an inter-comparison between the IBBCEAS

196   of this study and the IBBCEAS of Cambridge University was conducted. The HONO measurements

197   from the two different instruments were highly correlated ($R^2 = 0.95$, Fig. 2c). In addition, the

198   IBBCEAS instrument was also compared with the long optical path absorption photometer (LOPAP)

199   and the stripping coil ion chromatography (SC-IC) in our previous studies (Tang et al., 2019;Duan et al.,

200   2018), which also showed good correlations for HONO measurements (LOPAP: $R^2 = 0.894$, SC-IC: R^2

201    $= 0.98$).

3 Results and discussion

3.1 General observations and vertical measurements

204   The time-series of meteorological parameters, NR-PM$_1$ mass concentration, HONO, NO$_x$ and

205   other relevant species are shown in Fig. 3. Based on the NR-PM$_1$ mass concentration level, three

206   different meteorological conditions were characterized during the measurement period (Table 1). The

207 first episode (E1) from 7 December to 10:00 on 8 December was a haze event. NR-PM$_1$ mass

208 concentration increased rapidly from 30 to ~150 µg·m^{-3} at ground level and 260 m on the tower due to

209 a low wind speed (0.78 ± 0.42 m·s^{-1}) and high RH (51% ± 13%).

210  The second episode (8-11 December, C2) was a clean event with low NR-PM$_1$ mass loading

211 (mean: 24 ± 19 µg·m^{-3}), high wind speed (> 5 m·s^{-1}) dominantly from northwest. The third episode (E3)

212 from 11 December to 12 December was another haze event. During this period, characterized by

213 stagnant weather, lower wind speeds (an average of 0.77 ± 0.4 m·s^{-1}), and high RH (55% ± 5%). The

214 mass concentration of NR-PM$_1$ gradually increased and then remained at relatively constant levels at

215 ground level and 260 m on the tower, and ranging from 69 to 218 µg·m^{-3} with the mean value of 154 ±

216 35 µg·m^{-3}.

217  Throughout the entire measurement period, HONO concentrations ranged from 0.05 to 7.59 ppb.

218 The mean HONO mixing ratios during E1, C2, and E3 were 4.26 ± 2.08, 0.83 ± 0.65, and 3.54 ± 0.91

219 ppb, respectively. The maximum concentration of HONO was 7.59 ppb, which was observed during E1

220 (at 08:10 on 8 December). From 11 to 12 December, with stagnant weather, the pollutants continuously

221 increased. HONO concentrations remained a high level, and the daytime mean HONO mixing ratio

222 even reached 3.1 ± 0.92 ppb. Figure 3 also presents the time series of measured simultaneously other

223 relevant species. The mean NO$_2$ mixing ratios during E1, C2 and E3 were 51.98 ± 8.41, 23.30 ± 11.91,

224 and 51.88 ± 5.97 ppb, respectively. Because NO and O$_3$ were not measured at ground level after 14:00

225 on 10 December, the mean concentrations of NO and O$_3$ during E1 and C2 were 90.99 ± 67.98, 14.66 ±

226 21.79 ppb, and 4.04 ± 1.81, 14.37 ± 10.65 ppb, respectively. After sunset, the concentration of O$_3$ at the

227 surface was rapidly titrated by elevated NO and increased with the increase of height. The mixing ratio

228 of O$_3$ below 260 m was less than 9 ppb during the vertical measurements.

229  Nocturnal stable surface layers of air are generally formed at low wind speed (< 6 m·s^{-1})

230 (VandenBoer et al., 2013). Hence vertical profile data are adopted when wind speed was less than 6

231 m·s^{-1} except on 7 December (Fig. 4). Vertical measurements with low wind events were successfully

232 conducted in three occasions (9-10, 10-11, and 11-12 December) and would be discussed below. The

233 near-continuous vertical measurement avoids the observation bias from prolonged fixed sampling. The

234 date and time of measurement for each vertical profile is detailed in Table S1 in the Supplement.

3.2 Nocturnal HONO vertical profiles

3.2.1 Vertical measurements after sunset

Vertical measurements were conducted from ground level to 240 m after sunset. Figure 5 show the temporal and spatial variations of HONO and NO_2 during the clean episode (C2) and the haze episode (E3). The mixing ratios of HONO and NO_2 at ground level were consistent with those measured in the container, indicating that HONO and NO_2 were relatively well mixed during these two episodes.

The vertical profiles of HONO, NO_2, and $\triangle$HONO just after sunset are shown in Fig. 6. During C2 and E3, the mixing ratios of HONO and NO_2 (Fig. 6a) showed nearly flat profiles throughout the column. The vertical variations of $\triangle$HONO (Fig. 6b), which is the difference of HONO concentration between measured in the container and at ground level, centered around 0 ppb and varied between -0.4 and 0.4 ppb, confirming the relatively uniform vertical distribution of both HONO and NO_2. The vertical variations of T and RH during these three measurements were similar (Fig. S2). While T decreased gradually as the increase with increasing height, RH increased gradually with increasing height, and RH was relatively higher during the haze episode. Also, there were no T inversion just after sunset, and the consistent variations of HONO and NO_2 at ground level and vertical measurements supports a relatively well-mixed boundary layer, which explains the uniform vertical distribution of HONO and NO_2.

3.2.2 Nocturnal vertical profiles

Nocturnal small-scale stratification and layering was determined according to the method of Brown et al. (2012), who used the potential temperature profile as an indicator of atmospheric static stability. According to the vertical variations in potential temperature, the stable layer was divided into the "surface layer", the "nocturnal boundary layer (NBL)", the "top of the nocturnal boundary layer" and the "residual layer (RL)".

Figure 7 depicts the nocturnal vertical profiles of HONO, NO_2 and potential temperature during the clean episode. On the night of 9 December (C2), negative profiles of both HONO and NO_2 were clearly seen. When the container ascended during 22:42-23:06, the potential temperature profile showed distinct stratification. The surface layer extended to 10-20 m and the NBL extended to ~140 m. There was a significant negative gradient HONO within NBL. Above the NBL, a negative gradient of HONO was also observed in the RL but was not consistently observed in other measurements (see below). When the descent of the container during 23:15-23:40, the potential temperature profile

265   showed that a shallow T inversion was rapidly formed between 130 and 200 m. Within the shallow

266   inversion layer, the vertical convection and transport was inhibited, and the remarkable negative

267   gradient was observed there. Within the NBL, the negative gradient of HONO and NO_2, however,

268   disappeared. This might due to the continuous vertical mixing from 23:06 to 23:40. By the way, the

269   surface source of HONO is obvious as seen from the apparent accumulation of HONO within NBL. In

270   addition, the obviously vertical variation in RH during 23:15-23:40 (Fig. S3) indicated the different

271   layers at different height, which was due to the influence of the shallow inversion layer.

272   The vertical profile of potential temperature on 10 December (C2) shows that shallow inversion

273   layer formed between the surface layer and the NBL. In the shallow inversion layer, the mixing ratios

274   of HONO decreased rapidly with increasing height, and a significant negative gradient was observed

275   within the shallow inversion layer and surface layer. With the attenuation of the shallow inversion layer

276   during the descent of the container from 23:01 to 23:25, the inhibition of vertical transport and mixing

277   gradually weakened, and the negative gradient of HONO disappeared below ~100 m, which indicated

278   the surface source of HONO or the interaction of different air masses due to the change of WD (Fig.

279   S3). And the attenuation event of shallow inversion layer may also be the result of the increase of wind

280   speed and interaction of different air masses that changed from the west to southeast between 15 and

281   100 m. Above 100 m height, the mixing ratio of HONO decreased with increasing height, and the

282   fluctuation of HONO likely due to the interaction of different air masses. In contrast, the vertical

283   profile of NO_2 shows that NO_2 rapidly decreased towards the ground; a significant positive gradient

284   was observed near the surface, which was caused by several factors. The nocturnal NO_2 is produced by

285   the reaction of O_3 with NO, which mainly occurs near the surface, resulting in a negative gradient in

286   NO_2. However, this effect was counteracted by the dry deposition of NO_2, which by itself would result

287   in a positive gradient (Stutz et al., 2004b). Meanwhile, the mixing ratio of NO_2 was also affected by

288   local traffic emission sources. All of these lead to the positive gradient of NO_2 near the surface.

289   Compared to the vertical profiles collected on 9 December, a near-surface shallow inversion layer was

290   formed on 10 December, resulting in the clearly positive gradient of near-surface NO_2. Moreover, the

291   increase of the positive gradient of NO_2 indicates the formation of near-surface shallow inversion layer

292   likely caused the increase of dry deposition, which affects the vertical distribution of HONO and NO_2

293   at night.

294   Although the surface layer was a common feature in the potential temperature profiles, it was

295   absent on the night of 11-12 December (E3), and the NBL extended downward to the lowest

296   measurement height (8 m above the ground; Fig. 8). With the development of the boundary layer, the

297   negative gradient of HONO and NO_2 gradually disappeared during 22:35-23:29, which was similar to

298   the vertical profile on 9 December. As shown in Fig. 8, the vertical profile of HONO showed a

299   significant negative gradient as the container ascent during 22:35-23:00, and higher HONO mixing

300   ratios were observed at ground level. However, the mixing ratios of HONO and NO_2 approached a

301   steady-state plateau within NBL around midnight. A possible physical and chemical process, the loss of

302   HONO to the ground surface by dry deposition and vertical convection could account for approaching

303   a near-steady states in the HONO mixing ratio and HONO/NO_2 (Fig. S4). Similar vertical

304   measurements were reported by VandenBoer et al (2013) who also observed a near-steady state in the

305   HONO mixing ratio and HONO/NO_2. Dry deposition loss of HONO to the ground surface and vertical

306   mixing effects associated with vertical convection reached a near-steady state around midnight, which

307   indicated that significant quantities of HONO are deposited to the ground surface at night, and

308   deposition of HONO at ground surface is an important sink of HONO at night.

309   **3.3 Direct emission**

310   In the present study, the measurement site is surrounded by several main roads, and thus might be

311   affected by substantial vehicle emissions at night. To evaluate the influence of direct emissions,

312   emission ratios of HONO/NO_x was derived from our measurement. Since NO was not measured at

313   ground level after 10 December, the nocturnal measurement data of HONO and NO_x (18:00-6:00) from

314   9 November to 10 December were used to evaluate the local HONO emission factor. Considering the

315   differences in the type of vehicles, fuel compositions, etc., the reported emission factor of HONO/NO_x

316   might not be representative for Beijing region. In order to evaluate the influence of direct emission, the

317   local emission factor of HONO was estimated from the ambient measurements.

318   As an air mass becomes aged, the conversion of NO_2 to HONO will result in the increase of

319   HONO/NO_x; freshly emitted air masses are characterized by the lowest HONO/NO_x. Thus, the

320   observed minimum HONO/NO_x could be used as an upper limit for the emission factor (Li et al.,

321   2012;Su et al., 2008a). In order to capture as much of the freshly emitted air mass as possible, two

322   criteria were chosen to ensure that the air mass was dominated by fresh vehicle emission: (a) NO≥80

323   ppb and (b) NO/NO_x≥80% (Xu et al., 2015). The derived HONO/NO_x of 1.41% is comparable to the

324   value of 1.24% reported by Liang et al. (2017), who measured HONO emission factor in a road tunnel

325   in Hong Kong. $HONO_{emis}$ was calculated by the following equation: $[HONO]_{emis} = 0.0141 \times [NO_x]$.

326   The frequency distribution of $HONO_{emission}$/HONO during the measurement period is shown in Fig. S5.

327   The contribution of direct emissions to ambient HONO was estimated to be 51.1%, suggesting that

328   vehicle emissions is an important nocturnal HONO source in Beijing (Zhang et al., 2018).

329   **3.4 Nocturnal HONO chemistry**

330   **3.4.1 Correlation studies**

331   The heterogeneous conversion of NO_2 is an important pathway of HONO formation as many field

332   measurements have also found a strong correlation between HONO and NO_2 (Zhou et al., 2006;Su et

333   al., 2008a;Wang et al., 2013;Huang et al., 2017). However, the use of correlation analysis to interpret

334   the heterogeneous conversion of NO_2 should be carefully treated, as physical transport and source

335   emissions also contribute to the correlation. In this study, the correlation of vertical measurements

336   between HONO and NO_2 were analyzed. Vertical profile data without horizontal transport were used to

337   avoid the influence of physical transport. As shown in Fig. 9, HONO and NO_2 exhibited moderate but

338   significant correlations (C2: $R^2 = 0.72$, E3: $R^2 = 0.69$), indicating that NO_2 participated in the formation

339   of HONO.

340   The adsorbed water on the surface affects the heterogeneous formation of HONO (Stutz et al.,

341   2004a). The relationship between HONO/NO_2 and RH is illustrated in Fig. 10. Following the method

342   introduced by Stutz et al (2004a), we analyzed the average of the five highest HONO/NO_2 value in

343   each 10% RH interval to eliminate much of the influence of factors like the time of night, advection,

344   the surface density, etc. An increase in the HONO/NO_2 ratio along with RH was observed at each

345   height interval when RH was less than 70%. Previous observation at ground level also reported that the

346   HONO/NO_2 ratio increased with the increase of RH when RH was less than 70%, while the further

347   increase of RH would lead to decrease in the HONO/NO_2, which may be caused by an increase in the

348   number of water layers formed on the surface with the increase of RH, resulting in the more efficient

349   uptake of HONO (Li et al., 2012;Wang et al., 2013b;Yu et al., 2009). The HONO/NO_2 ratio decreased

350   with the increase of height at similar RH level for both C2 and E3, which implied that the ground

351   surface was the main heterogeneous reaction surface at night. It is important to note that the limited

352   vertical measurements result in the limited variation range of RH, which limits the analysis. Additional

353   efforts are needed to conduct more comprehensive vertical measurements to interpret the HONO/NO$_2$

354   ratios versus RH for different height in the future.

355   **3.4.2 Influence of aerosol surface on nocturnal HONO production**

356   The relative importance of aerosol surfaces and ground surfaces in nocturnal HONO production

357   has been widely investigated in the field (Kleffmann et al., 2003;Oswald et al., 2015;VandenBoer et al.,

358   2013;Stutz, 2002;Wong et al., 2011;Ye et al., 2018;Li et al., 2012;Su et al., 2008a). An estimate of the

359   contribution of nocturnal HONO production from aerosol surfaces, we can expect that the air mass in

360   the RL (above 200 m) is less affected by the ground-level processes (Brown et al., 2012; VandenBoer et

361   al., 2013). It can be approximately considered that the HONO production was primarily derived from

362   the heterogeneous conversion of NO$_2$ on aerosol surfaces, HONO production (*P(HONO)*) can then be

363   expressed using the following equation:

364
$$\frac{P(HONO)}{[NO_2]} = \frac{1}{4} \times \left[\frac{s}{v}\right] \times \sqrt{\frac{8RT}{\pi M}} \times \gamma \qquad (1)$$

365   where γ is the uptake coefficient of NO$_2$, R is the gas constant, T is the absolute temperature (K), M is

366   the molecular mass of NO$_2$ (M=4.6×10^{-2} kg mol^{-1}), and $\left[\frac{s}{v}\right]$ is the aerosol surface area density (m^{-1}).

367   The NO$_2$-normalized HONO production over time, $\Delta\frac{[HONO]}{[NO_2]}/\Delta t$, can be calculated using Eq. (2):

368
$$\Delta\frac{[HONO]}{[NO_2]}/\Delta t \sim \frac{1}{4} \times \left[\frac{s}{v}\right] \times \sqrt{\frac{8RT}{\pi M}} \times \gamma \qquad (2)$$

369   Assuming that the uptake coefficient of NO$_2$ is 1×10^{-5}, which fits NO$_2$ uptake coefficient value of

370   1×10^{-6}-1×10^{-5} from those observed in relevant studies (J.Kleffmanna et al., 1998;Kurtenbach et al.,

371   2001;George et al., 2005;Stemmler et al., 2007), with a $\left[\frac{s}{v}\right]$ value of ~10^{-3} m^{-1} (Wang et al., 2018). A

372   relative HONO formation rate of $\Delta\frac{[HONO]}{[NO_2]}/\Delta t$ is ~0.0032 h^{-1}, which is equivalent to the HONO

373   production of 0.17 ppb h^{-1} when the upper limit of observed nocturnal NO$_2$ above 200 m was 52.9 ppb

374   during E3. The nocturnal accumulation of HONO (18:00-00:00) in the RL (above 200 m) is 1.02 ppb

375   during E3, which is much less than the HONO vertical measurements of 3.06 ppb. It is necessary to

376   elaborate that: (1) the typical $\left[\frac{s}{v}\right]$ is ~10^{-3} m^{-1} during the pollution period in winter in Beijing (NO$_2$=

377   45 ppb, temperature = 273 K); (2) the upper limit of NO$_2$ uptake coefficient and the upper limit of

378   observed nocturnal NO$_2$ in the RL are used to calculate the HONO production on aerosol. The HONO

379   production could be actually overestimated in our study. As described, HONO production from the

380 heterogeneous conversion of NO_2 solely on the aerosol surfaces cannot explain HONO vertical

381 measurements at night. In addition, the integrated column of HONO ($HONO_{column}$) and the mixing

382 ratios of HONO observed from ground level to 10 m height ($HONO_{ground}$) show a significant

383 correlation ($R^2 = 0.85$) (Fig. 11), which also indicates that the ground surface is the primary reaction

384 surface on which HONO is formed, and then transported throughout the column.

385 **3.4.3 Nocturnal HONO production at ground level**

386 The nocturnal HONO in the boundary layer is primarily derived from the heterogeneous

387 conversion from NO_2 to HONO on the ground surface, which is consistent with the results of other

388 studies in vertical gradient of HONO (Kleffmann et al., 2003;Wong et al., 2011;Zhang et al., 2009;Ye et

389 al., 2018). The conversion rate of NO_2 can be evaluated using the HONO conversion frequency.

390 However, real atmospheric components are affected by physical processes, chemical processes, and

391 direct emissions. To reduce the uncertainties associated with transport process and source emissions,

392 the HONO conversion frequency was calculated using the scaling method proposed by Su et al (2008)

393 and adopting NO_2 and BC as reference species. Before calculation, the HONO concentration was

394 corrected by direct emission (Eq. (3)). Because NO was not measured at ground level after 14:00 on 10

395 December, the data of NO_x was not available during the vertical measurements at night on 10 and 11

396 December. The monthly average $HONO_{emis}$/HONO ratio of 51.1% was calculated to correct the

397 observed HONO ($HONO_{corr}$). The HONO conversion frequency C_{HONO} can be expressed as:

398
$$[HONO]_{corr} = [HONO] - [HONO]_{emis} = [HONO] - [HONO] \times 0.511 \tag{3}$$

399
$$C_{HONO}^X = \frac{2\left(\frac{[HONO_{corr}]_{t_2} \times [\overline{X}]}{[X]_{t_2}} - \frac{[HONO_{corr}]_{t_1} \times [\overline{X}]}{[X]_{t_1}}\right)}{(t_2 - t_1)\left(\frac{[NO_2]_{t_2}}{[X]_{t_2}} + \frac{[NO_2]_{t_1}}{[X]_{t_1}}\right)[\overline{X}]}$$

400
$$= \frac{2\left(\frac{[HONO_{corr}]_{t_2}}{[X]_{t_2}} - \frac{[HONO_{corr}]_{t_1}}{[X]_{t_1}}\right)}{(t_2 - t_1)\left(\frac{[NO_2]_{t_2}}{[X]_{t_2}} + \frac{[NO_2]_{t_1}}{[X]_{t_1}}\right)} \tag{4}$$

401
$$C_{HONO} = \frac{1}{3}\left(C_{HONO}^0 + C_{HONO}^{NO_2} + C_{HONO}^{BC}\right) \tag{5}$$

402 where $[HONO_{corr}]_t$, $[NO_2]_t$, and $[X]_t$ represent mixing ratios of HONO, NO_2, and the reference gas

403 at the sampling time t, C_{HONO} is average conversion frequency, C_{HONO}^X is the conversion frequency

404 scaled with species X, and C_{HONO}^0 is the conversion frequency which is not scaled. The average

405 conversion frequencies C_{HONO} on 9, 10 and 11 December were 0.0039 h^{-1}, 0.0026 h^{-1}, and 0.0039 h^{-1},

406 respectively, which was comparable to the observations of Hou et al. (2016) in Beijing (the clean

407   episode: 0.0065 h⁻¹; the haze episode:0.0039 h⁻¹) and Lammel et al. (1996) in Mainz and Milan (0.0041

408   h⁻¹ and 0.00491 h⁻¹), but much lower than observations made by Li et al. (2012) (0.024 h⁻¹) and Su et al.

409   (2008) (0.016 h⁻¹) at a rural site in southern China.

410   As illustrated above, HONO production from the heterogeneous conversion of NO_2 on the aerosol

411   surfaces cannot explain our HONO vertical measurements. The heterogeneous conversion from NO_2 to

412   HONO on ground surfaces at nighttime was further evaluated,

413
$$C_{HONO} = \frac{P_{HONO}}{[NO_2]} = \frac{\phi_{NO_2 \to HONO} \times v_{NO_2}^{ground}}{H} - \frac{v_{HONO}^{ground}}{H} \times \frac{[HONO_{corr}]}{[NO_2]} \qquad (6)$$

414   where v_{HONO}^{ground} and $v_{NO_2}^{ground}$ are the dry deposition velocities of HONO and NO_2, which were

415   expected to be similar since the nocturnal controlling resistances were mainly the aerodynamic

416   resistance and the quasi-laminar layer resistance (Su et al., 2008a; Stutz et al., 2002). $\phi_{NO_2 \to HONO}$ is

417   the HONO yield from deposited NO_2, which varies between 0 and 1, indicating that the deposited NO_2

418   molecule is not necessarily converted to HONO. *H* is the mixing depth.

419   Previous studies reported the value of v_{HONO}^{ground} between 0.077 and 3 cm s⁻¹ (Harrison and Kitto,

420   1994;Harrison et al., 1996;Spindler et al., 1998;Stutz, 2002;Coe and Gallagher, 1992). In the present

421   study, we used a mean v_{HONO}^{ground} of 0.095 cm s⁻¹ (Su et al., 2008a;Stutz, 2002;Coe and Gallagher, 1992)

422   and assumed that boundary layer mixing depth H is 100 m high. The $\phi_{NO_2 \to HONO}$ values on 9 (C2), 10

423   (C2) and 11 December (E3) were 0.10, 0.08, and 0.09, respectively, which means that every 10-13

424   deposited NO_2 molecules will result in one HONO being released into atmosphere. The value of

425   deposited NO_2 molecules converted into gas phase HONO is within the range of published results

426   (3-33) (Stutz et al., 2002; Su et al., 2008a; Li et al., 2012). The derived $\phi_{NO_2 \to HONO}$ value is lower

427   than calculation by Su et al (2008a) (0.34), which is caused by the differences in surface environment

428   between urban and rural areas. Similar $\phi_{NO_2 \to HONO}$ values were found during C2 and E3, suggesting

429   that the potential of heterogeneous conversion from NO_2 to HONO on ground surface at night is

430   consistent.

431   **4 Conclusions**

432   High-resolution vertical profiles of HONO and NO_2 were measured using an IBBCEAS

433   instrument during the APHH-Beijing winter campaign. Although the data set of this study is rather

434   limited in scope, encompassing only four nights in December 2016 with a limited set of ancillary data,

435   it is unique because, to our knowledge, this is the first high-resolution vertical measurements of HONO

436   and NO_2 in urban areas of China. The observed HONO concentrations during E1, C2, and E3 were 4.26

437    $\pm$ 2.08, 0.83 $\pm$ 0.65, and 3.54 $\pm$ 0.91 ppb, respectively. The vertical distribution of HONO is consistent

438   with reduced mixing and stratification in the lower several hundred meters of the nocturnal urban

439   atmosphere. The $HONO_{emis}$/HONO ratio was 51.1%, indicating that direct emissions from combustion

440   processes have a great deal of influence on ambient HONO concentrations and is an important

441   nocturnal HONO sources at the measurement site. In addition, high-resolution vertical profiles of

442   HONO, HONO production from the heterogeneous conversion of NO_2 on aerosol surfaces cannot

443   explain HONO vertical measurements and the correlation between the integrated column of HONO and

444   HONO measured from the surface to 10 m height, all suggesting that the heterogeneous conversion of

445   NO_2 on the ground surface dominated the HONO production at night, and then transported throughout

446   the column due to the vertical convection.

447   A relatively well-mixed boundary layer was observed after sunset, and the △HONO fluctuated

448   around zero. The small-scale stratification of the nocturnal urban atmosphere and the formation of a

449   shallow inversion layer affect the vertical distribution of HONO and NO_2. The high-resolution vertical

450   profiles showed that dry deposition loss of HONO to the ground surface and vertical mixing effects

451   reached a near-steady state on the nighttime of 11-12 December, which revealed (1) the ground surface

452   is the dominant reaction surface on which HONO is formed from the heterogeneous conversion of NO_2;

453   (2) significant quantities of HONO are deposited to the ground surface at night, which is an important

454   nocturnal sink of HONO. The nocturnal HONO production from the heterogeneous reaction of NO_2 at

455   ground level was evaluated, and the $\phi_{NO_2 \rightarrow HONO}$ values on 9 (C2), 10 (C2) and 11 December (E3)

456   were 0.10, 0.08 and 0.09, respectively. The similar values of $\phi_{NO_2 \rightarrow HONO}$ indicate that the potential of

457   heterogeneous conversion from NO_2 to HONO at the ground level is consistent for both the clean and

458   the haze episodes. Because of the relatively few vertical measurement cases and the limited height of

459   the meteorological tower, future vertical measurements of HONO to a high height (e.g., using tethered

460   balloons) and more comprehensive vertical measurements in the megacities, are urgently needed for a

461   better understanding of the vertical distribution and the formation mechanisms of HONO in the PBL in

462   megacities.

463

464   *Data availability*. The data used in this study are available from the corresponding author upon request

465   (mqin@aiofm.ac.cn).

466

Supplement.

468

Author contributions. MQ and PX organized the field contributions from Anhui Institute of Optics and Fine Mechanics group for the APHH-Beijing project. MQ and JD designed the research. WF and JD built the IBBCEAS instrument. JD and KT conducted the measurements. FM and MQ analyzed the data. FM wrote the paper. MQ, YS and CY revised and commented on the paper.

473

Competing interests. The authors declare that they have no conflict of interest.

475

Special issue statement. This article is part of the special issue "In-depth study of air pollution sources and processes within Beijing and its surrounding region (APHH-Beijing) (ACP/AMT inter-journal SI)". It is not associated with a conference.

479

Acknowledgements. This work was supported by the National Natural Science Foundation of China (91544104, 41571130023, 41875154), the National Key R&D Program of China (2017YFC0209400, 2016YFC0208204), and the Science and Technology Major Special Project of Anhui Province, China (16030801120).

483

484

References

Acker, K., Febo, A., Trick, S., Perrino, C., Bruno, P., Wiesen, P., Möller, D., Wieprecht, W., Auel, R., Giusto, M., Geyer, A., Platt, U., and Allegrini, I.: Nitrous acid in the urban area of Rome, Atmos. Environ., 40, 3123-3133, https://doi.org/10.1016/j.atmosenv.2006.01.028, 2006.

Alicke, B., Platt, U., Stutz, J.: Impact of nitrous acid photolysis on the total hydroxyl radical budget during the Limitation of Oxidant Production/Pianura Padana Produzione di Ozono study in Milan, J. Geophys. Res., 107, LOP 9-1-LOP 9-17, https://doi.org/10.1029/2000jd000075, 2002.

An, J., Li, Y., Chen, Y., Li, J., Qu, Y., and Tang, Y. J.: Enhancements of major aerosol components due to additional HONO sources in the North China Plain and implications for visibility and haze, Adv. Atmos. Sci., 30, 57-66, https://doi.org/10.1007/s00376-012-2016-9, 2012.

Aubin, D. G., and Abbatt, J. P. D.: Interaction of NO_2 with Hydrocarbon Soot: Focus on HONO Yield, Surface Modification, and Mechanism, J. Phys. Chem. A., 111, 6263-6273, https://doi.org/10.1021/jp068884h, 2007.

Bao, F. X., Li, M., Zhang, Y., Chen, C. C., and Zhao, J. C.: Photochemical Aging of Beijing Urban $PM_{2.5}$: HONO Production, Environ. Sci. Technol., 52, 6309-6316, https://doi.org/10.1021/acs.est.8b00538, 2018.

Bartolomei, V., Alvarez, E. G., Wittmer, J., Tlili, S., Strekowski, R., Temime-Roussel, B., Quivet, E., Wortham, H.,

500   Zetzsch, C., Kleffmann, J., and Gligorovski, S.: Combustion Processes as a Source of High Levels of Indoor
501   Hydroxyl Radicals through the Photolysis of Nitrous Acid, Environ. Sci. Technol., 49, 6599-6607,
502   https://doi.org/10.1021/acs.est.5b01905, 2015.

503   Bejan, I., Abd-El-Aal, Y., Barnes, I., Benter, T., Bohn, B., Wiesen, P., and Kleffmann, J.: The photolysis of
504   *ortho*-nitrophenols: a new gas phase source of HONO, Phys. Chem. Chem. Phys., 8, 2028-2035,
505   https://doi.org/10.1039/b516590c, 2006.

506   Brown, S. S., Dubé, W. P., Osthoff, H. D., Wolfe, D. E., Angevine, W. M., and Ravishankara, A. R.: High
507   resolution vertical distributions of NO_3 and N_2O_5 through the nocturnal boundary layer, Atmos. Chem. Phys., 7,
508   139-149, https://doi.org/10.5194/acp-7-139-2007, 2007.

509   Cai, R. L., Yang, D. S., Fu, Y. Y., Wang, X., Li, X. X., Ma, Y., Hao, J. M., Zheng, J., and Jiang, J. K.: Aerosol
510   surface area concentration: a governing factor in new particle formation in Beijing, Atmos. Chem. Phys., 17,
511   12327-12340, https://doi.org/ /10.5194/acp-17-12327-2017, 2017.

512   Coe, H., and Gallagher, M. W.: Measurements of Dry Deposition of NO_2 to A Dutch Heathland Using the
513   Eddy-Correlation Technique, Q. J. Roy. Meteor. Soc., 118, 767-786, https://doi.org/10.1002/qj.49711850608, 1992.

514   Cui, L. L., Li, R., Zhang, Y. C., Meng, Y., Fu, H. B. and Chen, J. M.: An observational study of nitrous acid
515   (HONO) in Shanghai, China: The aerosol impact on HONO formation during the haze episodes, Sci. Total
516   Environ., 630, 1057-1070, https://doi.org/10.1016/j.scitotenv.2018.02.063, 2018.

517   Duan, J., Qin, M., Ouyang, B., Fang, W., Li, X., Lu, K. D., Tang, K., Liang, S. X., Meng, F. H., Hu, Z. K., Xie, P.
518   H., Liu, W. Q., and Häsler, R.: Development of an incoherent broadband cavity-enhanced absorption spectrometer
519   for in situ measurements of HONO and NO_2, Atmos. Meas. Tech., 11, 4531-4543,
520   https://doi.org/10.5194/amt-11-4531-2018, 2018.

521   Finlayson-Pitts, B. J., Wingen, L. M., Sumner, A. L., Syomin, D., and Ramazan, K. A.: The heterogeneous
522   hydrolysis of NO_2 in laboratory systems and in outdoor and indoor atmospheres: An integrated mechanism, Phys.
523   Chem. Chem. Phys., 5, 223-242, https://doi.org/10.1039/b208564j, 2003.

524   Fu, X., Wang, T., Zhang, L., Li, Q. Y., Wang, Z., Xia, M., Yun, H., Wang, W. H., Yu, C., Yue, D. L., Zhou, Y.,
525   Zheng, J. Y., and Han, R.: The significant contribution of HONO to secondary pollutants during a severe winter
526   pollution event in southern China, Atmos. Chem. Phys., 19, 1-14, https://doi.org/10.5194/acp-19-1-2019, 2019.

527   George, C., Strekowski, R. S., Kleffmann, J., Stemmler, K., and Ammann, M.: Photoenhanced uptake of gaseous
528   NO_2 on solid organic compounds: a photochemical source of HONO?, Faraday Discuss., 130, 195-210,
529   https://doi.org/10.1039/b417888m, 2005.

530   Gómez Alvarez, E., Sörgel, M., Gligorovski, S., Bassil, S., Bartolomei, V., Coulomb, B., Zetzsch, C., and Wortham,
531   H.: Light-induced nitrous acid (HONO) production from NO_2 heterogeneous reactions on household chemicals,
532   Atmos. Environ., 95, 391-399, https://doi.org/10.1016/j.atmosenv.2014.06.034, 2014.

533   Han, C., Yang, W. J., Wu, Q. Q., Yang, H., and Xue, X. X.: Heterogeneous Photochemical Conversion of NO_2 to
534   HONO on the Humic Acid Surface under Simulated Sunlight, Environ. Sci. Technol., 50, 5017-5023,
535   https://doi.org/10.1021/acs.est.5b05101, 2016.

536   Han, C., Yang, W. J., Yang, H., and Xue, X. X.: Enhanced photochemical conversion of NO_2 to HONO on humic
537   acids in the presence of benzophenone, Environ. Pollut., 231, 979-986,
538   https://doi.org/10.1016/j.envpol.2017.08.107, 2017.

539   Hanst, P. L., Spence, J. W., and Miller, M.: Atmospheric Chemistry of N-nitroso Dimethylamine, Environ. Sci.
540   Technol., 11, 403-405, https://doi.org/10.1021/es60127a007, 1977.

541   Harrison, R. M., and Kitto, A. M. N.: Evidence for a surface source of atmospheric nitrous acid, Atmos. Environ.,
542   28, 1089-1094, https://doi.org/10.1016/1352-2310(94)90286-0, 1994.

543   Harrison, R. M., Peak, J. D., and Collins, G. M.: Tropospheric cycle of nitrous acid, J. Geophys. Res., 101,

544   14429-14439, https://doi.org/10.1029/96JD00341, 1996.

545   Hendrick, F., Müller, J. F., Clémer, K., Wang, P., De Mazière, M., Fayt, C., Gielen, C., Hermans, C., Ma, J. Z.,

546   Pinardi, G., Stavrakou, T., Vlemmix, T., and Van Roozendael, M.: Four years of ground-based MAX-DOAS

547   observations of HONO and NO_2 in the Beijing area, Atmos. Chem. Phys., 14, 765-781,

548   https://doi.org/10.5194/acp-14-765-2014, 2014.

549   Hou, S. Q., Tong, S. R., Ge, M. F., and An, J. L.: Comparison of atmospheric nitrous acid during severe haze and

550   clean periods in Beijing, China, Atmos. Environ., 124, 199-206, https://doi.org/10.1016/j.atmosenv.2015.06.023,

551   2016.

552   Huang, R. J., Zhang, Y. L., Bozzetti, C., Ho, K. F., Cao, J. J., Han, Y. M., Daellenbach, K. R., Slowik, J. G., Platt, S.

553   M., Canonaco, F., Zotter, P., Wolf, R., Pieber, S. M., Bruns, E. A., Crippa, M., Ciarelli, G., Piazzalunga, A.,

554   Schwikowski, M., Abbaszade, G., Schnelle-Kreis, J., Zimmermann, R., An, Z. S., Szidat, S., Baltensperger, U., El

555   Haddad, I., and Prévôt, A. S. H.: High secondary aerosol contribution to particulate pollution during haze events in

556   China, Nature, 514, 218-222, https://doi.org/10.1038/nature13774, 2014.

557   Huang, R. J., Yang, L., Cao, J. J., Wang, Q. Y., Tie, X. X., Ho, K. F., Shen, Z. X., Zhang, R. J., Li, G. H., Zhu, C. S.,

558   Zhang, N. N., Dai, W. T., Zhou, J. M., Liu, S. X., Chen, Y., Chen, J., and O'Dowd, C. D.: Concentration and

559   sources of atmospheric nitrous acid (HONO) at an urban site in Western China, Sci. Total Environ., 593-594,

560   165-172, https://doi.org/10.1016/j.scitotenv.2017.02.166, 2017.

561   Hao, N., Zhou, B., Chen, D., and Chen, L. M..: Observations of nitrous acid and its relative humidity dependence

562   in Shanghai, J. Environ. Sci., 18, 910-915, https://doi.org/10.1016/S1001-0742(06)60013-2, 2006.

563   Kleffmanna, J., Beckera, K. H., and Wiesena, P.: Heterogeneous NO_2 conversion processes on acid surfaces:

564   possible atmospheric implications, Atmos. Environ., 32, 2721-2729,

565   https://doi.org/10.1016/S1352-2310(98)00065-X, 1998.

566   Karamchandani, P., Emery, C., Yarwood, G., Lefer, B., Stutz, J., Couzo, E., and Vizuete, W.: Implementation and

567   refinement of a surface model for heterogeneous HONO formation in a 3-D chemical transport model, Atmos.

568   Environ., 112, 356-368, https://doi.org/10.1016/j.atmosenv.2015.01.046, 2015.

569   Kleffmann, J., Becker, K. H., Lackhoff, M., and Wiesen, P.: Heterogeneous conversion of NO_2 on carbonaceous

570   surfaces, Phys. Chem. Chem. Phys., 1, 5443-5450, https://doi.org/10.1039/A905545B, 1999.

571   Kleffmann, J., Kurtenbach, R., Lörzer, J., Wiesen, P., Kalthoff, N., Vogel, B., and Vogel, H.: Measured and

572   simulated vertical profiles of nitrous acid—Part I: Field measurements, Atmos. Environ., 37, 2949-2955,

573   https://doi.org/10.1016/s1352-2310(03)00242-5, 2003.

574   Kleffmann, J.: Daytime Sources of Nitrous acid (HONO) in the Atmospheric Boundary Layer, Chemphyschem, 8,

575   1137-1144, https://doi.org/10.1002/cphc.200700016, 2007.

576   Kurtenbach, R., Becker, K. H., Gomes, J. A. G., Kleffmann, J., Lörzer, J., Spittler, M., Wiesen, P., Ackermann, R.,

577   Geyer, A., and Platt, U.: Investigations of emission and heterogeneous formation of HONO in a road traffic tunnel,

578   Atmos. Environ., 35, 3385–3394, https://doi.org/10.1016/S1352-2310(01)00138-8, 2001.

579   Laufs, S., Cazaunau, M., Stella, P., Kurtenbach, R., Cellier, P., Mellouki, A., Loubet, B., and Kleffmann, J.: Diurnal

580   fluxes of HONO above a crop rotation, Atmos. Chem. Phys., 17, 6907-6923,

581   https://doi.org/10.5194/acp-17-6907-2017, 2017.

582   Li, S. P., Matthews, J., and Sinha, A.: Atmospheric Hydroxyl Radical Production from Electronically Excited NO_2

583   and H_2O, Science, 319, 1657-1660, https://doi.org/10.1126/science.1151443, 2008.

584   Li, X., Brauers, T., Häseler, R., Bohn, B., Fuchs, H., Hofzumahaus, A., Holland, F., Lou, S., Lu, K. D., Rohrer, F.,

585   Hu, M., Zeng, L. M., Zhang, Y. H., Garland, R. M., Su, H., Nowak, A., Wiedensohler, A., Takegawa, N., Shao, M.,

586   and Wahner, A.: Exploring the atmospheric chemistry of nitrous acid (HONO) at a rural site in Southern China,

587   Atmos. Chem. Phys., 12, 1497-1513, https://doi.org/10.5194/acp-12-1497-2012, 2012.

588 Li, X., Rohrer, F., Hofzumahaus, A., Brauers, T., Häseler, R., Bohn, B., Broch, S., Fuchs, H., Gomm, H., Holland,
589 F., Jäger, J., Kaiser, J., Keutsch, F. N., Lohse, I., Lu, K. D., Tillmann, R., Wegener, R., Wolfe, G. M., Mentel, T. F.,
590 Kiendler-Scharr, A., Wahner, A.: Missing Gas-Phase Source of HONO Inferred from Zeppelin Measurement in the
591 Troposphere, Science, 334, 292-296, https://doi.org/10.1126/science.1248999, 2014.

592 Liang, Y. T., Zha, Q. Z., Wang, W. H., Cui, L., Lui, K. H., Ho, K. F., Wang, Z., Lee, S. C., and Wang, T.: Revisiting
593 nitrous acid (HONO) emission from on-road vehicles: A tunnel study with a mixed fleet, J. Air Waste Manag., 67,
594 797-805, https://doi.org/10.1080/10962247.2017.1293573, 2017.

595 Liu, Y. H., Lu, K. D., Li, X., Dong, H. B., Tan, Z. F., Wang, H. C., Zou, Q., Wu, Y. S., Zeng, L. M., Hu, M., Min, K.
596 E., Kecorius, S., Wiedensohler, A., and Zhang, Y. H.: A Comprehensive Model Test of the HONO Sources
597 Constrained to Field Measurements at Rural North China Plain, Environ. Sci. Technol., 53, 3517-3525,
598 https://doi.org/10.1021/acs.est.8b06367, 2019.

599 Liu, Z., Wang, Y. h., Costabile, F., Amoroso, A., Zhao, C., Huey, L. G., Stickel, R., Liao, J., and Zhu, T.: Evidence
600 of Aerosols as a Media for Rapid Daytime HONO Production over China, Environ. Sci. Technol., 48, 14386-14391,
601 https://doi.org/10.1021/es504163z, 2014.

602 Liu, Z., Wang, Y., Gu, D., Zhao, C., Huey, L. G., Stickel, R., Liao, J., Shao, M., Zhu, T., Zeng, L., Amoroso, A.,
603 Costabile, F., Chang, C.-C., and Liu, S.-C.: Summertime photochemistry during CAREBeijing-2007:RO_x budgets
604 and O_3 formation, Atmos. Chem. Phys., 12, 7737-7752, https://doi.org/10.5194/acp-12-7737-2012, 2012.

605 Lu, K. D., Rohrer, F., Holland, F., Fuchs, H., Bohn, B., Brauers, T., Chang, C. C., Häseler, R., Hu, M., Kita, K.,
606 Kondo, Y., Li, X., Lou, S. R., Nehr, S., Shao, M., Zeng, L. M., Wahner, A., Zhang, Y. H., and Hofzumahaus, A.:
607 Observation and modelling of OH and HO_2 concentrations in the Pearl River Delta 2006: a missing OH source in a
608 VOC rich atmosphere, Atmos. Chem. Phys., 12, 1541-1569, https://doi.org/10.5194/acp-12-1541-2012, 2012.

609 Ma, Q. X., Wang, T., Liu, C., He, H., Wang, Z., Wang, W. H., and Liang, Y. T.: SO_2 Initiates the Efficient
610 Conversion of NO_2 to HONO on MgO Surface, Environ. Sci. Technol., 51, 3767-3775,
611 https://doi.org/10.1021/acs.est.6b05724, 2017.

612 Mendez, M., Blond, N., Amedro, D., Hauglustaine, D. A., Blondeau, P., Afif, C., Fittschen, C., and Schoemaecker,
613 C.: Assessment of indoor HONO formation mechanisms based on in situ measurements and modeling, Indoor Air,
614 27, 443-451, https://doi.org/10.1111/ina.12320, 2017.

615 Meusel, H., Kuhn, U., Reiffs, A., Mallik, C., Harder, H., Martinez, M., Schuladen, J., Bohn, B., Parchatka, U.,
616 Crowley, J. N., Fischer, H., Tomsche, L., Novelli, A., Hoffmann, T., Janssen, R. H. H., Hartogensis, O., Pikridas,
617 M., Vrekoussis, M., Bourtsoukidis, E., Weber, B., Lelieveld, J., Williams, J., Pöschl, U., Cheng, Y. F., and Su, H.:
618 Daytime formation of nitrous acid at a coastal remote site in Cyprus indicating a common ground source of
619 atmospheric HONO and NO, Atmos. Chem. Phys., 16, 14475-14493, https://doi.org/10.5194/acp-16-14475-2016,
620 2016.

621 Michoud, V., Colomb, A., Borbon, A., Miet, K., Beekmann, M., Camredon, M., Aumont, B., Perrier, S., Zapf, P.,
622 Siour, G., Ait-Helal, W., Afif, C., Kukui, A., Furger, M., Dupont, J. C., Haeffelin, M., and Doussin, J. F.: Study of
623 the unknown HONO daytime source at a European suburban site during the MEGAPOLI summer and winter field
624 campaigns, Atmos. Chem. Phys., 14, 2805-2822, https://doi.org/10.5194/acp-14-2805-2014, 2014.

625 Michoud, V., Doussin, J.-F., Colomb, A., Afif, C., Borbon, A., Camredon, M., Aumont, B., Legrand, M., and
626 Beekmann, M.: Strong HONO formation in a suburban site during snowy days, Atmos. Environ., 116, 155-158,
627 https://doi.org/10.1016/j.atmosenv.2015.06.040, 2015.

628 Monge, M. E., D'Anna, B., Mazri, L., Giroir-Fendler, A., Ammann, M., Donaldson, D. J., and George, C.: Light
629 changes the atmospheric reactivity of soot, P. Natl. Acad. Sci. USA, 107, 6605-6609,
630 https://doi.org/10.1073/pnas.0908341107, 2010.

631 Neuman, J. A., Trainer, M., Brown, S. S., Min, K. E., Nowak, J. B., Parrish, D. D., Peischl, J., Pollack, I. B.,

632   Roberts, J. M., Ryerson, T. B., and Veres, P. R.: HONO emission and production determined from airborne
633   measurements over the Southeast U.S, J. Geophys. Res.-Atmos., 121, 9237-9250,
634   https://doi.org/10.1002/2016JD025197, 2016.

635   Oswald, R., Behrendt, T., Ermel, M., Wu, D., Su, H., Cheng, Y., Breuninger, C., Moravek, A., Mougin, E., Delon,
636   C., Loubet, B., Pommerening-Röser, A., Sörgel, M., Pöschl, U., Hoffmann, T., Andreae, M. O., Meixner, F. X. and
637   Trebs, I.: HONO Emissions from Soil Bacteria as a Major source of Atmospheric Reactive Nitrogen, Science, 341,
638   1233-1235, https://doi.org/10.1126/science.1242266, 2013.

639   Oswald, R., Ermel, M., Hens, K., Novelli, A., Ouwersloot, H. G., Paasonen, P., Petäjä, T., Sipilä, M., Keronen, P.,
640   Bäck, J., Königstedt, R., Hosaynali Beygi, Z., Fischer, H., Bohn, B., Kubistin, D., Harder, H., Martinez, M.,
641   Williams, J., Hoffmann, T., Trebs, I., and Sörgel, M.: A comparison of HONO budgets for two measurement
642   heights at a field station within the boreal forest in Finland, Atmos. Chem. Phys., 15, 799-813,
643   https://doi.org/10.5194/acp-15-799-2015, 2015.

644   Pitts, J. N., Grosjean, D., Cauwenberghe, K. V., Schmid, J. P., and Fitz, D. R.: Photooxidation of aliphatic amines
645   under simulated atmospheric conditions: formation of nitrosamines, nitramines, amides, and photochemical
646   oxidant, Environ. Sci. Technol., 12, 946-953, https://doi.org/10.1021/es60144a009, 1978.

647   Bröske, R., Kleffmann, J., and Wiesen, P.: Heterogeneous conversion of NO_2 on secondary organic aerosol
648   surfaces: A possible source of nitrous acid (HONO) in the atmosphere?, Atmos. Chem. Phys., 3, 469-474,
649   https://doi.org/10.5194/acp-3-469-2003, 2003.

650   Reisinger, A. R.: Observations of HNO_2 in the polluted winter atmosphere: possible heterogeneous production on
651   aerosols, Atmos. Environ., 34, 3865-3874, https://doi.org/10.1016/S1352-2310(00)00179-5, 2000.

652   Scharko, N. K., Martin, E. T., Losovyj, Y., Peters, D. G., and Raff, J. D.: Evidence for Quinone Redox Chemistry
653   Mediating Daytime and Nighttime NO_2-to-HONO Conversion on Soil Surfaces, Environ. Sci. Technol., 51,
654   9633-9643, https://doi.org/10.1021/acs.est.7b01363, 2017.

655   Sleiman, M., Gundel, L. A., Pankow, J. F., Jacob III, P., Singer, B. C., and Destaillats, H.: Formation of
656   carcinogens indoors by surface-mediated reactions of nicotine with nitrous acid, leading to potential thirdhand
657   smoke hazards, P. Natl. Acad. Sci. USA, 107, 6576-6581, https://doi.org/10.1073/pnas.0912820107, 2010.

658   Sörgel, M., Regelin, E., Bozem, H., Diesch, J. M., Drewnick, F., Fischer, H., Harder, H., Held, A.,
659   Hosaynali-Beygi, Z., Martinez, M., and Zetzsch, C.: Quantification of the unknown HONO daytime source and its
660   relation to NO_2, Atmos. Chem. Phys., 11, 10433-10447, https://doi.org/10.5194/acp-11-10433-2011, 2011.

661   Spataro, F., Ianniello, A., Esposito, G., Allegrini, I., Zhu, T., and Hu, M.: Occurrence of atmospheric nitrous acid in
662   the urban area of Beijing (China), Sci. Total Environ., 447, 210-224,
663   https://doi.org/10.1016/j.scitotenv.2012.12.065, 2013.

664   Spindler, G., Brüggemann, E., and Herrmann, H.: Nitrous acid (HNO_2) Concentration Measurements and
665   Estimation of Dry Deposition over Grassland in Eastern Germany, Transactions on Ecology and Environment, 28,
666   223-227, 1999.

667   Stemmler, K., Ammann, M., Donders, C., Kleffmann, J., and George, C.: Photosensitized reduction of nitrogen
668   dioxide on humic acid as a source of nitrous acid, Nature, 440, 195-198, https://doi.org/10.1038/nature04603,
669   2006.

670   Stemmler, K., Ndour, M., Elshorbany, Y., Kleffmann, J., D'Anna, B., George, C., Bohn, B., and Ammann, M.:
671   Light induced conversion of nitrogen dioxide into nitrous acid on submicron humic acid aerosol, Atmos. Chem.
672   Phys., 7, 4237-4248, https://doi.org/10.5194/acp-7-4237-2007, 2007.

673   Stutz, J., Alicke, B., Neftel, A.: Nitrous acid formation in the urban atmosphere: Gradient measurements of NO_2
674   and HONO over grass in Milan, Italy, J. Geophys. Res., 107, LOP 5-1-LOP 5-15,
675   https://doi.org/10.1029/2001JD000390, 2002.

676   Stutz, J., Alicke, B., Ackermann, R., Geyer, A., Wang, S. H., White, A. B., Williams, E. J., Spicer, C. W., and Fast,

677   J. D.: Relative humidity dependence of HONO chemistry in urban areas, J. Geophys. Res.-Atmos., 109, D03307,

678   https://doi.org/10.1029/2003JD004135, 2004a.

679   Stutz, J., Alicke, B., Ackermann, R., Geyer, A., White, A., and Williams, E.: Vertical profiles of NO$_3$, N$_2$O$_5$, O$_3$,

680   and NO$_x$ in the nocturnal boundary layer: 1. Observations during the Texas Air Quality Study 2000, J. Geophys.l

681   Res.-Atmos., 109, D12306, https://doi.org/10.1029/2003JD004209, 2004b.

682   Su, H., Cheng, Y. F., Cheng, P., Zhang, Y. H., Dong, S. F., Zeng, L. M., Wang, X. S., Slanina, J., Shao, M., and

683   Wiedensohler, A.: Observation of nighttime nitrous acid (HONO) formation at a non-urban site during

684   PRIDE-PRD2004 in China, Atmos. Environ., 42, 6219-6232, https://doi.org/10.1016/j.atmosenv.2008.04.006,

685   2008a.

686   Su, H., Cheng, Y. F., Shao, M., Gao, D. F., Yu, Z. Y., Zeng, L. M., Slanina, J., Zhang, Y. H., and Wiedensohler, A.:

687   Nitrous acid (HONO) and its daytime sources at a rural site during the 2004 PRIDE-PRD experiment in China, J.

688   Geophys. Res., 113, D14312, https://doi.org/10.1029/2007JD009060, 2008b.

689   Su, H., Cheng, Y. F., Oswald, R., Behrendt, T., Trebs, I., Meixner, F. X., Andreae, M. O., Cheng, P., Zhang, Y. H.,

690   and Pöschl, U.: Soil nitrite as a Source of Atmospheric HONO and OH Radicals, Science, 333, 1616-1618,

691   https://doi.org/10.1126/science.1207687, 2011.

692   Sun, Y. L., Wang, Z. F., Fu, P. Q., Yang, T., Jiang, Q., Dong, H. B., Li, J., and Jia, J. J.: Aerosol composition,

693   sources and processes during wintertime in Beijing, China, Atmos. Chem. Phys., 13, 4577-4592,

694   https://doi.org/10.5194/acp-13-4577-2013, 2013.

695   Tang, K., Qin, M., Duan, J., Fang, W., Meng, F. H., Liang, S. X., Xie, P. H., Liu, J. G., Liu, W. Q., Xue, C. Y., and

696   Mu, Y. J.: A dual dynamic chamber system based on IBBCEAS for measuring fluxes of nitrous acid in agricultural

697   fields in the North China Plain, Atmos. Environ., 196, 10-19, https://doi.org/10.1016/j.atmosenv.2018.09.059,

698   2019.

699   Tang, Y., An, J., Wang, F., Li, Y., Qu, Y., Chen, Y., and Lin, J.: Impacts of an unknown daytime HONO source on

700   the mixing ratio and budget of HONO, and hydroxyl, hydroperoxyl, and organic peroxy radicals, in the coastal

701   regions of China, Atmos. Chem. Phys., 15, 9381-9398, https://doi.org/10.5194/acp-15-9381-2015, 2015.

702   Tong, S. R., Hou, S. Q., Zhang, Y., Chu, B. W., Liu, Y. C., He, H., Zhao, P. S., and Ge, M. F.: Exploring the nitrous

703   acid (HONO) formation mechanism in winter Beijing: direct emissions and heterogeneous production in urban and

704   suburban areas, Faraday Discuss., 189, 213-230, https://doi.org/10.1039/c5fd00163c, 2016.

705   VandenBoer, T. C., Brown, S. S., Murphy, J. G., Keene, W. C., Young, C. J., Pszenny, A. A. P., Kim, S., Warneke,

706   C., de Gouw, J. A., Maben, J. R., Wagner, N. L., Riedel, T. P., Thornton, J. A., Wolfe, D. E., Dubé, W. P., Öztürk, F.,

707   Brock, C. A., Grossberg, N., Lefer, B., Lerner, B., Middlebrook, A. M., and Roberts, J. M.: Understanding the role

708   of the ground surface in HONO vertical structure: High resolution vertical profiles during NACHTT-11, J. Geophy.

709   Res.- Atmos., 118, 10155-110171, https://doi.org/10.1002/jgrd.50721, 2013.

710   Villena, G., Kleffmann, J., Kurtenbach, R., Wiesen, P., Lissi, E., Rubio, M. A., Croxatto, G., and Rappenglück, B.:

711   Vertical gradients of HONO, NO$_x$ and O$_3$ in Santiago de Chile, Atmos. Environ., 45, 3867-3873,

712   https://doi.org/10.1016/j.atmosenv.2011.01.073, 2011.

713   Vogel, B., Vogel H., Kleffmann, J., and Kurtenbach, R.: Measured and simulated vertical profiles of nitrous

714   acid—Part II. Model simulations and indications for a photolytic source, Atmos. Environ., 37, 2957-2966,

715   https://doi.org/10.1016/S1352-2310(03)00243-7, 2003.

716   Wang, H. C., Lu, K. D., Chen, X. R., Zhu, Q. D., Wu, Z. J., Wu, Y. S., and Sun, K.: Fast particulate nitrate

717   formation via N$_2$O$_5$ uptake aloft in winter in Beijing, Atmos. Chem. Phys., 18, 10483-10495,

718   https://doi.org/10.5194/acp-18-10483-2018, 2018.

719   Wang, J. Q., Zhang, X. S., Guo, J., Wang, Z. W., and Zhang, M. G.: Observation of nitrous acid (HONO) in Beijing,

720 China: Seasonal variation, nocturnal formation and daytime budget, Sci. Total Environ., 587-588, 350-359,

721 https://doi.org/10.1016/j.scitotenv.2017.02.159, 2017.

722 Wang, S. S., Zhou, R., Zhao, H., Wang, Z. R., Chen, L. M., and Zhou, B.: Long-term observation of atmospheric

723 nitrous acid (HONO) and its implication to local NO_2 levels in Shanghai, China, Atmos. Environ., 77, 718-724,

724 https://doi.org/10.1016/j.atmosenv.2013.05.071, 2013.

725 Wong, K. W., Oh, H. -J., Lefer, B. L., Rappenglück, B., and Stutz, J.: Vertical profiles of nitrous acid in the

726 nocturnal urban atmosphere of Houston, TX, Atmos. Chem. Phys., 11, 3595-3609,

727 https://doi.org/10.5194/acp-11-3595-2011, 2011.

728 Wong, K. W., Tsai, C., Lefer, B., Haman, C., Grossberg, N., Brune, W. H., Ren, X., Luke, W., and Stutz, J.:

729 Daytime HONO vertical gradients during SHARP 2009 in Houston, TX, Atmos. Chem. Phys., 12, 635-652,

730 https://doi.org/10.5194/acp-12-635-2012, 2012.

731 Wong, K. W., Tsai, C., Lefer, B., Grossberg, N., and Stutz, J.: Modeling of daytime HONO vertical gradients

732 during SHARP 2009, Atmos. Chem. Phys., 13, 3587-3601, https://doi.org/10.5194/acp-13-3587-2013, 2013.

733 Xu, W. Q., Sun, Y. L., Wang, Q. Q., Zhao, J., Wang, J. F., Ge, X. L., Xie, C. H., Zhou, W., Du, W., Li, J., Fu, P. Q.,

734 Wang, Z. F., Worsnop, D. R., and Coe, H.: Changes in Aerosol Chemistry From 2014 to 2016 in Winter in Beijing:

735 Insights From High-Resolution Aerosol Mass Spectrometry, J. Geophys. Res.- Atmos., 124, 1132-1147,

736 https://doi.org/10.1029/2018JD029245, 2019.

737 Xu, Z., Wang, T., Wu, J. Q., Xue, L. K., Chan, J., Zha, Q., Z., Zhou, S. Z., Louie, P. K. K., and Luk, C. W. Y.:

738 Nitrous acid (HONO) in a polluted subtropical atmosphere: Seasonal variability, direct vehicle emissions and

739 heterogeneous production at ground surface, Atmos. Environ., 106, 100-109,

740 https://doi.org/10.1016/j.atmosenv.2015.01.061, 2015.

741 Ye, C. X., Zhang, N., Gao, H. L., and Zhou, X. L.: Photolysis of Particulate Nitrate as a Source of HONO and NO_x,

742 Environ. Sci. Technol., 51, 6849-6856, https://doi.org/10.1021/acs.est.7b00387, 2017.

743 Ye, C. X., Zhou, X. L., Pu, D., Stutz, J., Festa, J., Spolaor, M., Tsai, C., Cantrell, C., Mauldin III, R. L.,

744 Weinheimer, A., Hornbrook, R. S., Apel, E. C., Guenther, A., Kaser, L., Yuan, B., Karl, T., Haggerty, J., Hall, S.,

745 Ullmann, K., Smith, J., and Ortega, J.: Tropospheric HONO distribution and chemistry in the southeastern US,

746 Atmos. Chem. Phys., 18, 9107-9120, https://doi.org/10.5194/acp-18-9107-2018, 2018.

747 Yu, Y., Galle, B., Panday, A., Hodson, E., Prinn, R., and Wang, S.: Observations of high rates of NO_2-HONO

748 conversion in the nocturnal atmospheric boundary layer in Kathmandu, Nepal, Atmos. Chem. Phys., 9, 6401-6415,

749 https://doi.org/10.5194/acp-9-6401-2009, 2009.

750 Zhang, N., Zhou, X. L., Shepson, P. B., Gao, H. L., Alaghmand, M., and Stirm, B.: Aircraft measurement of

751 HONO vertical profiles over a forested region, Geophys. Res. Lett., 36, L15820,

752 https://doi.org/10.1029/2009GL038999, 2009.

753 Zhang, R., Wang, G., Guo, S., Zamora, M. L., Ying, Q., Lin, Y., Wang. W., Hu, M., and Wang, Y.: Formation of

754 Urban Fine Particulate Matter, Chem. Rev., 115, 3303-3855, https://doi.org/10.1021/acs.chemrev.5b00067, 2015.

755 Zhang, W. Q., Tong, S. R., Ge, M. F., An, J. L., Shi, Z. B., Hou, S. Q., Xia, K. H., Qu, Y., Zhang, H. X., Chu, B. W.,

756 Sun, Y. L., and He, H.: Variations and sources of nitrous acid (HONO) during a severe pollution episode in Beijing

757 in winter 2016, Sci. Total Environ., 648, 253-262, https://doi.org/10.1016/j.scitotenv.2018.08.133, 2018.

Table

Table 1 Classification of meteorological conditions and corresponding concentrations of NR-PM$_1$, NO$_2$ and HONO from 7 to 12 December

Time period	Weather condition	NR-PM$_1$ ($\mu g \cdot m^{-3}$)	HONO (ppb)	NO$_2$ (ppb)	WS (m·s^{-1})	WD	T (°C)	RH (%)
7 Dec - 8 Dec (10:00)	Haze (E1)	30-184	1.49-7.59	24.91-65.48	0.03-1.95	NW-ESE[a]	1.6-9.3	36-82
8 Dec (10:00) -11 Dec	Clean (C2)	3-97	0.05-3.75	3.33-47.84	0.01-6.24	NE-NW	-2.4-9.1	16-53
11 Dec - 12 Dec	Haze (E3)	69-217	1.54-5.51	38.58-66.57	0.02-1.81	NE-NW	-1.6-6.9	40-69

[a] NE: Northeast; ESE: East-southeast; NW: Northwest;

Figures
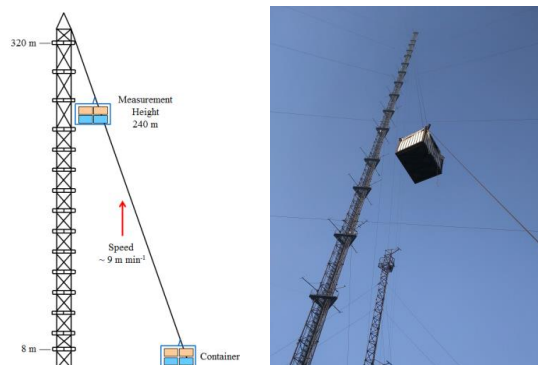
Figure 1. The Beijing 325-m meteorological tower (BMT) at the Institute of Atmospheric Physics (IAP).
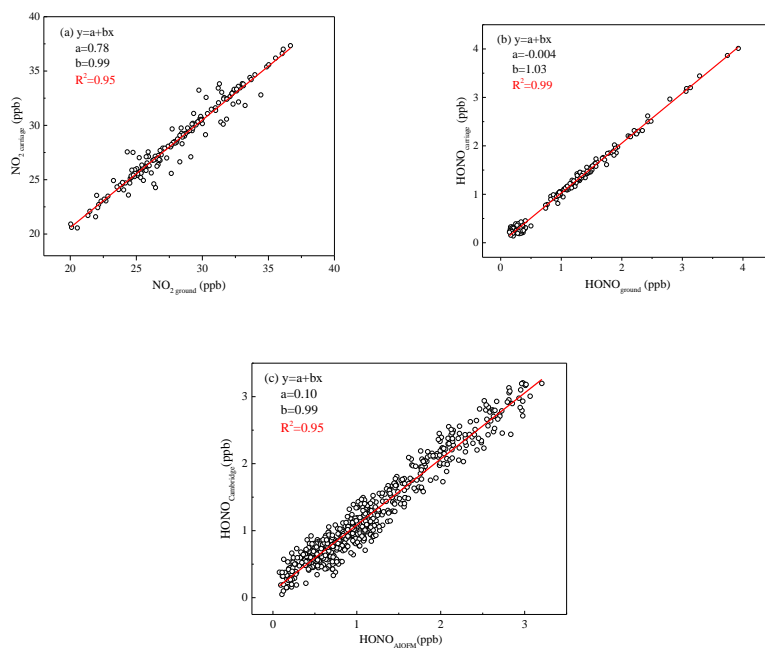
Figure 2. (a) Correlation of NO_2 concentration was measured by the two IBBCEAS instruments; (b) correlation of HONO concentration was measured by the two IBBCEAS instruments; (c) inter-comparison between the IBBCEAS of Cambridge university and the IBBCEAS of Anhui Institute of Optics and Fine Mechanics (AIOFM).
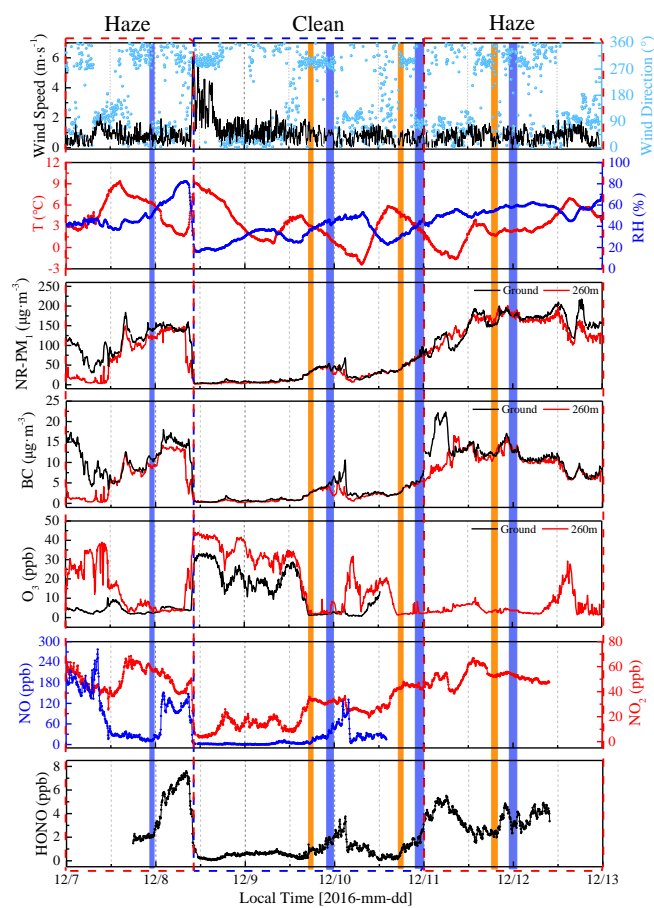
Figure 3. Time-series of wind speed (WS) and direction (WD), temperature (T), relative humidity (RH), NR-PM$_1$,

BC, O$_3$, NO, NO$_2$, and HONO from 7 to 12 December 2016 at IAP-Tower Division in Beijing, China. The

shaded region represents the eight vertical measurements (Table S1). The orange shaded region represents the

vertical measurements after sunset, and the violet shaded region represents the vertical measurements at night and

midnight.
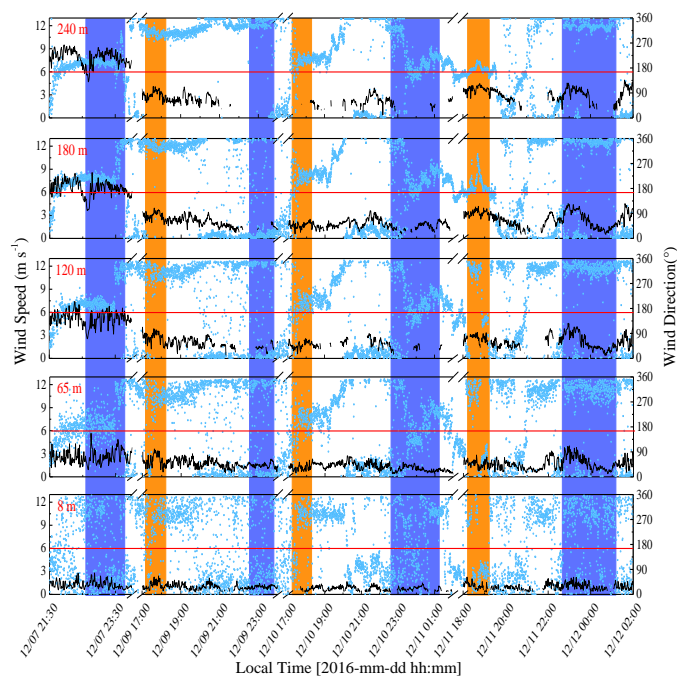
Figure 4. Temporal variations of the wind speed at fixed heights on the meteorological tower (8, 65, 120, 180, and 240 m) throughout the measurement period. Vertical measurements were conducted after sunset (orange shaded regions) and during nighttime (violet shaded regions). The red line denoted the wind speed is 6 m·s⁻¹.
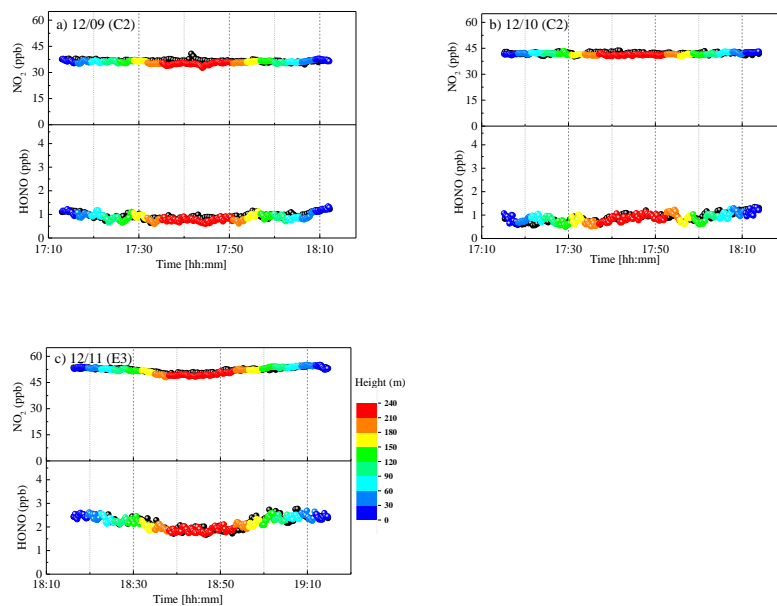
Figure 5. Temporal variations in the mixing ratios of HONO and NO$_2$ at ground level (black solid circles) and in the container (colored solid circles) during (a, b) the clean episode (C2) and (c) the haze episode (E3). The vertical measurements of HONO and NO$_2$ are color code by height.
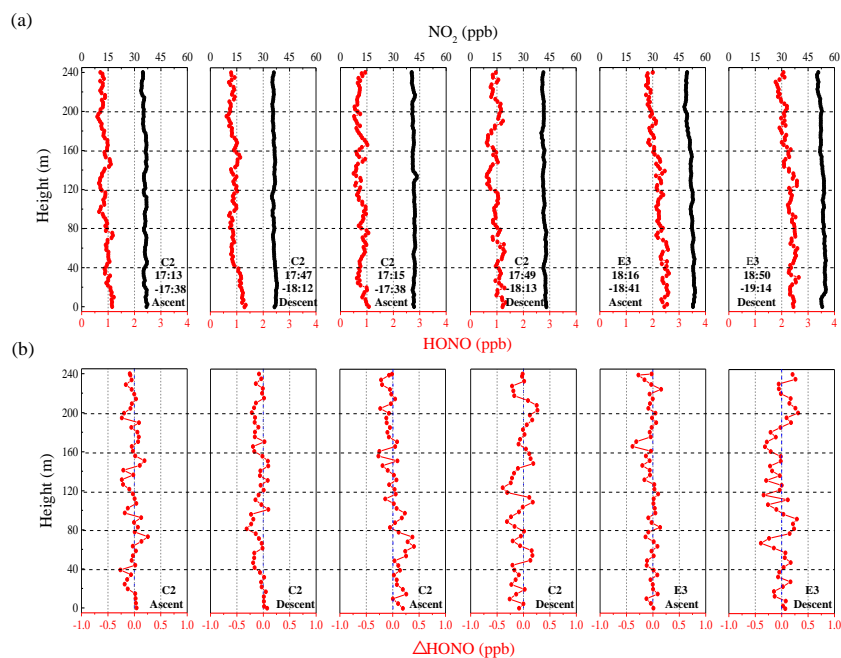
Figure 6. (a) Vertical profiles of HONO (red solid line) and NO₂ (black solid line) after sunset during the clean episode (C2) and the haze episode (E3). Each vertical measurement includes the ascent process and the descent process. The time on each plot corresponds to the measurement time of the vertical profile during the ascent or descent process. (b) Vertical profiles of △HONO (red dotted line) during C2 and E3 are also shown.
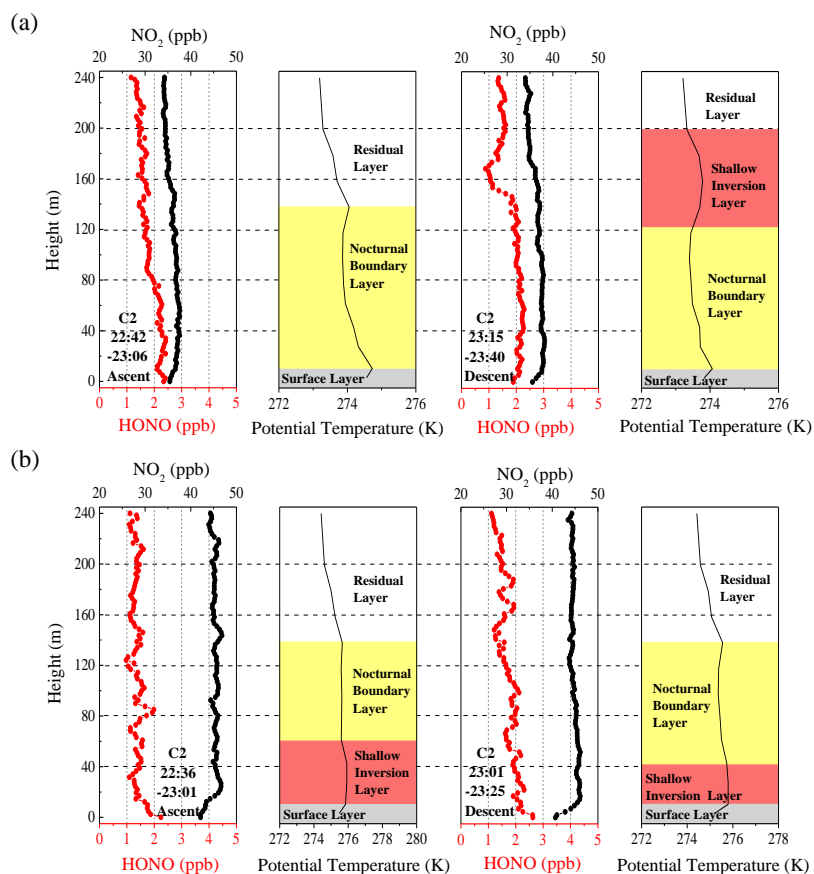
Figure 7. Nocturnal vertical profiles of HONO, NO₂ and potential temperature during the ascent and descent of the container on (a) 9 and (b) 10 December. The time in the figure corresponds to the measurement time of the vertical profile of HONO and NO₂. The different colors shaded region indicates the nocturnal small-scale stratification (surface layer, nocturnal boundary layer, shallow inversion layer and residual layer). The heights of the surface layer, shallow inversion layer, nocturnal boundary layer and residual layer are denoted by grey shaded regions, pink shaded regions, yellow shaded regions, and white shaded regions, respectively.
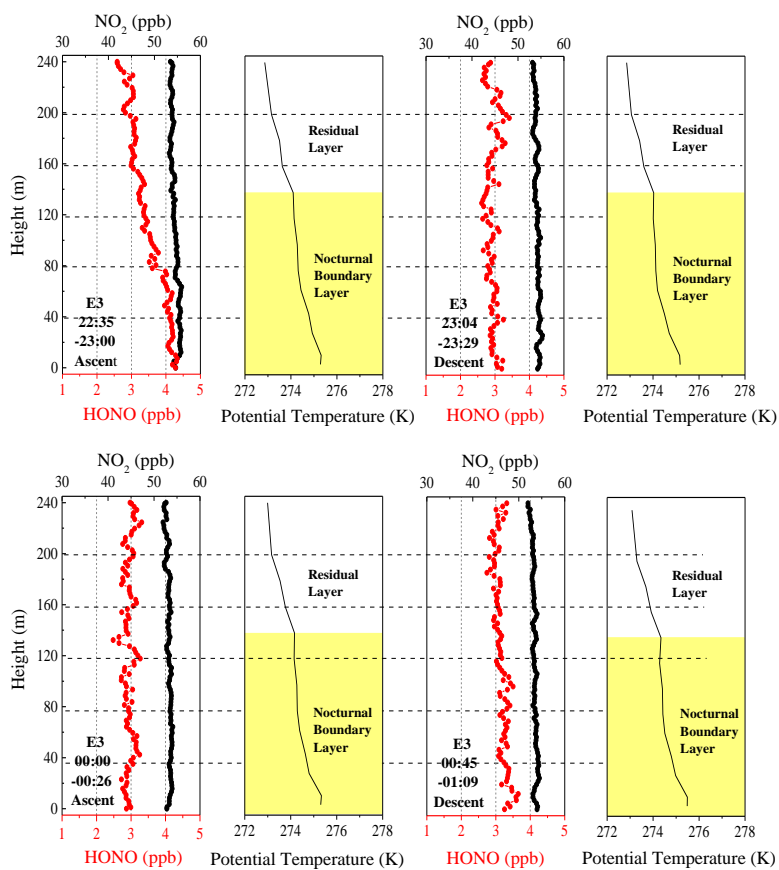
Figure 8. Vertical profiles of HONO and NO_2 on the night of 11 December and midnight of 12 December. The

potential temperature profiles indicate nocturnal small-scale stratification (nocturnal boundary layer and residual

layer). The height of the nocturnal boundary layer (NBL) is denoted by the yellow shaded region. The time in the

figure corresponds to the measurement time of the vertical profile of HONO and NO_2.
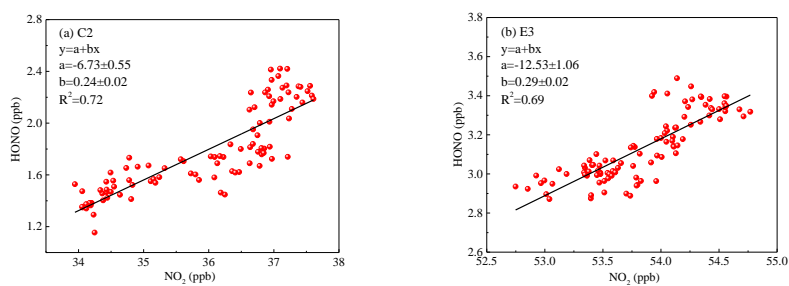
Figure 9. The correlation of the vertical profiles between HONO and NO_2 during (a) the clean episode (C2) and

(b) the haze episode (E3).
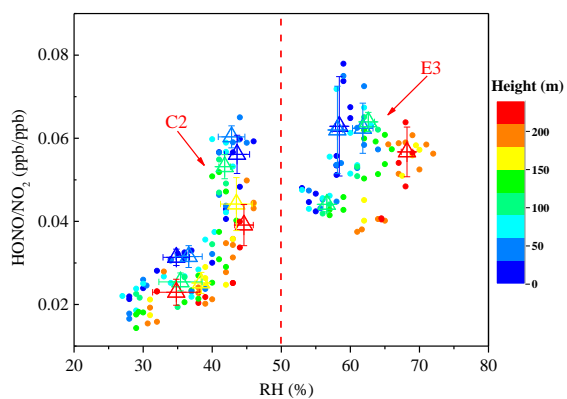
Figure 10. Scatter plot of HONO/NO_2 against RH of all vertical profiles during the clean episode (C2) and the

haze episode (E3). The HONO/NO_2 ratio is color coded by the heights. Triangles are the average of the first five

HONO/NO_2 value in each 10% RH interval at different height intervals (8-65 m, 65-120 m, 120-180 m and

180-240 m).
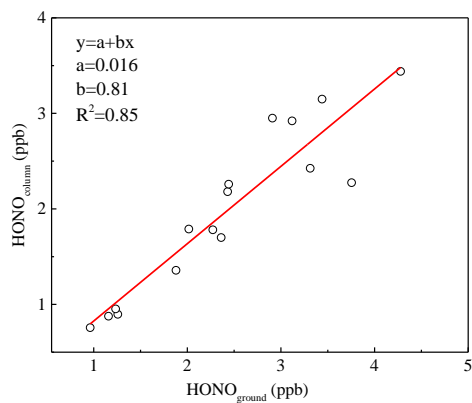
Figure 11. Correlation between the integrated column of HONO (10-240 m) and HONO measured from ground

level to 10 m above ground level (AGL). Column values of vertical measurements were calculated for 9 to 12

December.